International Journal of Mathematical Archive-6(3), 2015, 227-248
Available online through www.ijma.info ISSN 2229 – 5046

INFLUENCE OF HALL CURRENTS ON CROSS DIFFUSIVE CONVECTION IN A MHD BOUNDARY LAYER FLOW ON STRETCHING SHEET IN POROUS MEDIUM WITH HEAT GENERATION

G. Sarojamma*[1], Syed Mahaboobjan[2] and V. Nagendramma[3]

[1,2,3]Department of Applied Mathematics,
Sri Padmavati Women's University, Tirupati, Chittoor (Dt), India.

(Received On: 08-03-15; Revised & Accepted On: 31-03-15)

ABSTRACT

An analysis has been carried out to investigate the effects of Hall currents, heat absorption/generation, cross diffusion by the simultaneous action of mass flux due to temperature gradient (Soret effect) and heat flux (Dufour effect) in the boundary layer flow past a linearly stretching sheet embedded in a porous medium in the presence of thermal radiation and first order chemical reaction. The partial differential equations governing the flow are transformed into a set of coupled non – linear ordinary differential equations employing similarity variables which are solved numerically applying shooting technique with Runge – Kutta fourth order scheme. The results of the present analysis are compared with those available in literature and are found to be in good agreement. The numerical results pertaining to velocity, temperature and mass concentration distributions of the flow, the local skin friction coefficient, local Nusselt number and local Sherwood number are graphically presented and discussed for various governing parameters such as magnetic parameter, Hall parameter, porous parameter etc.,

Key words: *Hall Currents, MHD, Stretching Surface, Chemical Reaction, Heat Generation, Soret effect, Dufour effect.*

INTRODUCTION

Magnetic fields are abundantly utilized in several manufacturing processes such as MHD power generators, pumps and flow meters, in the design of cooling system, purification of molten metals from metallic inclusions with liquid metals etc. Recently the study of MHD flow and heat transfer gained significance due to its applications. For example, several metallurgical processes involve cooling of continuous filaments or strips. During this process these strips are stretched through a fluid. The quality of the end product depends on the rate of cooling. The rate of cooling of these final products with desired quality is accomplished by using electrically conducting fluids with applications of magnetic fields [1]. Several researchers [2-8] investigated the flow and heat transfer of electrically conducting fluids. In all these studies the Hall effect is ignored in the Ohm's law used. But Hall effects are of significant importance when the magnetic field is high. Abo – Eldahab and Salem [9] analyzed the effect of Hall currents on MHD convective flow of a power – law fluid past a stretching surface. Ali *et al.* [10] studied the MHD mixed convection boundary layer flow over a stretched vertical plate. In flows through porous media with combined buoyancy effects owing to heat and mass transfer, the coupling of heat and mass transfer takes place owing to the density variations with temperature and concentration. The direct coupling between temperature and concentration in possible when the cross diffusion Soret and Dufour effect is not small. When mass flux is produced due to temperature gradients it is known as Soret effect and Dufour effect refers to the heat flux by concentration gradients. Knobloch [11] and Taslim and Narusawa [12] explained the relation between Dufour and Soret numbers. Pal and Mondal[13] studied the combined effect of Soret and Dufour on unsteady MHD non – Darcy mixed convection over a

Corresponding Author: G. Sarojamma[1], [1,2,3]Department of Applied Mathematics,*
Sri Padmavati Women's University, Tirupati, Chittoor (Dt), India.

stretching sheet embedded in a saturated porous medium in the presence of thermal radiation, viscous dissipation and first – order chemical reaction. Anwar *et al.* [14] made a numerical study of MHD heat and mass transfer from a stretching surface in a porous medium with Soret and Dufour effects. Sallam[15] investigated the thermal-diffusion and diffusion-thermo effects on mixed convection heat and mass transfer in a porous medium. Kuznetsov and Nield[16] analyzed the double diffusive natural convective boundary layer flow of a nanofluid past a vertical plate. The analysis of heat and mass transfer due to chemical reaction is of great practical importance as many processes in several branches of science and technology. The engineering application involves chemical distillation process, formation and dispersion of fog, channel type solar energy collectors and thermo–protection systems. Chemical reaction can be classified as either heterogeneous or homogeneous process. This depends on whether they occur as a single phase volume reaction. A chemical reaction is said to be of first order, if the rate of reaction is directly proportional to the species concentration. Several studies Kandaswamy *et al.* [17], Mansour *et al.* [18], Takhar *et al.* [19] have been done. Nayak *et al.* [20] studied Soret and Dufour effects on mixed convection unsteady MHD boundary layer flow over stretching sheet in porous medium with chemically reactive species. Stanford Sateyi *et al.* [21] investigated the effect of Hall currents with Soret and Dufour effects on the flow on a vertical surface. In this analysis an attempts is made to study the effect of cross – diffusion and Hall current on the flow past a linearly stretching plate in the presence of heat generation / absorption, thermal radiation with first order chemical reaction.

MATHEMATICAL FORMULATION

Flow Analysis:

Consider the steady mixed convective flow of an incompressible viscous and electrically conducting fluid past a plate through a porous medium in the vertical direction stretching with a velocity proportional to the distance from the origin 'O' of a stationary frame of reference (x, y, z). The positive x coordinate is measured along the stretching sheet in the direction of motion and the positive y coordinate is measured normal to the sheet in the outward direction toward the fluid, the z-axis coincides with the leading edge of the stretching sheet.

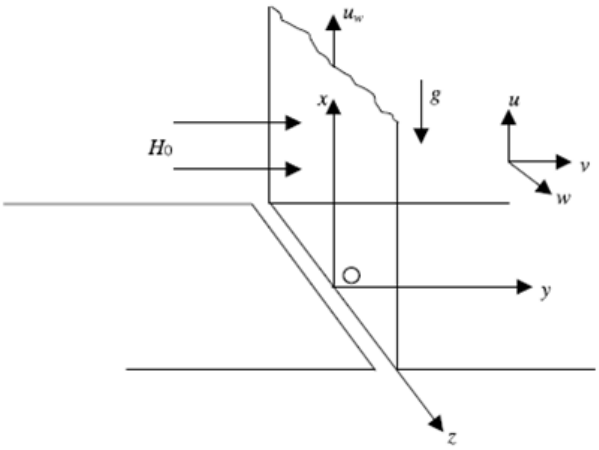

Fig. 1: Physical model and coordinate system

The Rosseland approximation is used to describe the radiative heat flux in the energy equation. The flow is subjected to a strong transverse magnetic field with a constant intensity B_0 along the positive y direction. The magnetic Reynolds is assumed to be small enough($Re < 1$), So that the induced magnetic field can be neglected. The governing equations for the magnetic field $\nabla \cdot \vec{H} = 0$, where $\vec{H} = (H_x, H_y, H_z)$ gives $H_z = H_0$ (constant) everywhere in the flow field, which gives $\vec{H} = (0, 0, H_0)$. If (J_x, J_y, J_z) are the component of electric current density $\vec{J}$, then the equation of conservation of electric charge $\nabla.\vec{J} = 0$ gives $J_z =$ constant. This constant is zero, that is, $J_z = 0$ everywhere in the flow since the plate is electrically non conducting. The generalized Ohm's law, in the absence of the electric field [22], is of the form

$$\vec{J} + \frac{\omega_e \tau_e}{H_0}\left(\vec{J} \times \vec{H}\right) = \sigma(\mu_e \vec{V} \times \vec{H} + \frac{1}{en_e}\nabla p_e) \quad (1)$$

where $\vec{V}, \sigma, \mu_e,\ \tau_e, e, n_e\ and\ p_e$ are the velocity, the electrical conductivity, the magnetic permeability, the cyclotron frequency, the electron collision time, the electric charge, the number density of the electron, and the electron pressure, respectively. Under the usual assumption, the electron pressure (for a weakly ionized gas), the thermoelectric pressure, and ion slip are negligible, so we have from the Ohm's law

$J_x + \omega_e \tau_e J_y = \sigma \mu_e H_0 v$

$J_y - \omega_e \tau_e J_x = -\sigma \mu_e H_0 v$

From which we obtain that

$$\left.\begin{aligned} J_x &= \frac{\sigma \mu_e H_0 (mu + v)}{1+m^2} \\ J_y &= \frac{\sigma \mu_e H_0 (mv - u)}{1+m^2} \end{aligned}\right\} \quad (2)$$

The flow has significant thermal radiation, chemical reaction, heat source, and Hall, Soret and Dufour effects. By using Boussinique approximation the basic boundary layer equations are given by

$$\frac{\partial u}{\partial y} + \frac{\partial v}{\partial y} = 0 \quad (3)$$

$$u\frac{\partial u}{\partial x} + v\frac{\partial u}{\partial y} = \vartheta \frac{\partial^2 u}{\partial y^2} + g\beta_T (T - T_\infty) + g\beta_c (C - C_\infty) - \frac{\sigma B_0^2}{\rho (1+m^2)}(u + mw) - \frac{\mu}{\rho k^*} u \quad (4)$$

$$u\frac{\partial w}{\partial x} + v\frac{\partial w}{\partial y} = \vartheta \frac{\partial^2 w}{\partial y^2} + \frac{\sigma B_0^2}{\rho (1+m^2)}(mu - w) - \frac{\mu}{\rho k^*} w \quad (5)$$

where u and v are velocity components in the x- direction and y – direction respectively, w is the velocity component in the z – direction. ϑ the kinematic coefficient of viscosity, g is the acceleration due to gravity, β_T is the coefficient of thermal expansion, T is the temperature of the fluid inside the thermal boundary layer, T_w is the plate temperature, T_∞ is the temperature of the fluid in the free stream with $T_w > T_\infty$, β_c is the volumetric coefficient of expansion with concentration, C is the fluid concentration, $\sigma (\sigma = \frac{e^2 n_e t_e}{m_e})$ is the electrical conductivity of the fluid, e is the electron charge, n_e is the electron number density, t_e is the electron collision time, m_e is the mass of electron, Bo is the Magnetic field of constant strength, ρ is the density of the fluid, m$(= w_e t_e)$ is the Hall parameter, $\omega_e \left(= e\frac{B_0}{m_e}\right)$ is the electron frequency, μ is the dynamic viscosity and k^* is the permeability of the porous medium.

The boundary conditions are

$$\left.\begin{aligned} u &= U_s = bx;\quad v = -v_w;\quad w = 0; && at\ y = 0 \\ u &\to 0,\ w \to 0 && as\ y \to \infty \end{aligned}\right\} \quad (6)$$

where U_s is the velocity of the surface, b is a constant with dimension $(time)^{-1}$ and v_w is the suction (> 0) or injection (> 0) of the velocity at the plate.

Introducing the similarity variables

$$u = bxf'(\eta),\ v = -\sqrt{bv} f(\eta),\quad w = bxg(\eta) \text{ and } \eta = \sqrt{\frac{b}{v}} y \quad (7)$$

Here $f(\eta)$ is the dimensionless stream function and η is the constant.

Substitution of the relations (7) in Eqs. (4) and (5) results in to the non – linear ordinary differential equations of the form

$$f''' + ff'' - f'^2 + \lambda\theta + \delta\phi - \frac{M}{(1+m^2)}(f' + mg) - \mathrm{k}_1 f' = 0 \quad (8)$$

$$g'' + fg' - f'g + \frac{M}{(1+m^2)}(mf' - g) + \mathrm{k}_1 g = 0 \quad (9)$$

Where M $= \frac{\sigma {B_0}^2}{\rho a}$ is the magnetic parameter, $\lambda = \frac{Gr_x}{Re_x^2}$ is the thermal buoyancy parameter,

Gr $= \frac{g\beta_T (T_w - T_\infty) x^3}{\nu^2}$ is the local thermal Grashof number, $\delta = \frac{Gc_x}{Re_x^2}$ is the solutal buoyancy parameter, Gc $= \frac{g\beta_c (C_w - C_\infty) x^3}{\nu^2}$ is the local Solutal Grashof number,$Re_x = \frac{\rho U_s}{\mu}$ is the Reynolds number, $\mathrm{k}_1 = \frac{\mu}{\rho b k^*}$ is the permeable parameter.

By using Eqs. (7) in Eqs. (6) the boundary conditions take the following non – dimensional form

$$\left.\begin{array}{ll} f'(\eta) = 1,\ f(\eta) = f_w\ ,\ g(\eta) = 0 & at\ \eta = 0 \\ f'(\eta) = 0, g(\eta) = 0 & as\ \eta \to \infty \end{array}\right\} \quad (10)$$

Where $f_w = \frac{v_w}{\sqrt{bv}}$ is the mass transfer coefficient such that $f_w > 0$ represents suction and $f_w < 0\ represents$ injection $at\ the\ surface$.

The local skin-friction coefficient C_{fx} along the x - direction is defined as

$$C_{fx} = \frac{2\tau_{wx}}{\rho(ax)^2} \quad (11)$$

The local skin – friction coefficients C_{fz} along the z - direction is defined as

$$C_{fz} = \frac{2\tau_{wz}}{\rho(ax)^2} \quad (12)$$

where τ_w is the wall sharing stress is given by $\tau_w = \mu(\frac{\partial u}{\partial y})_{y=0}$ (13)

By using the relations (7), Eqs. (11), (12) and (13) take the form

$$\left.\begin{array}{l} C_{fx}\mathrm{Re}_x^{-\frac{1}{2}} = 2f''(0) \quad and \\ C_{fz}\mathrm{Re}_x^{-1/2} = 2\mathrm{g}'(0) \end{array}\right\} \quad (14)$$

In the next section we consider the heat transfer in the flow using appropriate boundary conditions.

Heat transfer analysis:

Employing usual boundary layer approximations, the equation of the energy accounts for the heat generation/absorption, viscous dissipation and thermal radiation is given by

$$\rho c_p\left(u\frac{\partial T}{\partial x} + v\frac{\partial T}{\partial y}\right) = k\frac{\partial^2 T}{\partial y^2} + \frac{Dk_t}{C_s c_p}\frac{\partial^2 C}{\partial y^2} + \frac{\sigma B_0^2}{\rho(1+m^2)}(u^2 + w^2) - \frac{\partial q_r}{\partial y} + q''' \quad (15)$$

where K is the thermal conductivity, c_p is the specific heat at constant pressure, C_s is the concentration susceptibility, D is the mass diffusivity and k_t is the thermal - diffusion rate. The quantity q_r on the right hand side of equation (15) represents the radiative heat flux in the y-direction. Employing the Roseland diffusion approximation (Raptis [23]), the radiative heat flux is given by

$$q_r = -\frac{4\sigma^*}{3k^*}\frac{\partial T^4}{\partial y} \quad (16)$$

where σ^* is the Stephan – Boltzmann constant and k^* is the mass absorption coefficient, temperature differences within the flow are assumed to be sufficiently small so that T^4 may be expressed as a linear function of temperature T using a truncated Taylor series about the free stream temperature T_∞, i.e.,

$$T^4 = 4T_\infty^3 T - 3T_\infty^4. \quad (17)$$

From Eqs. (16) and (17), we obtain

$$\frac{\partial q_r}{\partial y} = -\frac{16\sigma^* T_\infty^3}{3K}\frac{\partial^2 T}{\partial y^2} \quad (18)$$

The coefficient q''' is the rate of internal heat generation ($> o$) or absorption(< 0).

The internal heat generation / absoption q''' is modeled (Dulal Pal [24]) as

$$q''' = \left(\frac{ku_s}{x\vartheta}\right)[A^*(T_w - T_\infty)f(\eta) + B^*(T - T_\infty)] \quad (19)$$

where $A^*$and B^* are coefficients of space-dependent and temperature – dependent internal heat generation or absorption respectively. It is noted that the case $A^* > 0$ and $B^* > 0$, corresponds to internal heat generation and that A^*<0 and $B^* < 0$, the case corresponds to internal heat absorption case.

The boundary conditions for temperature are

$$\left.\begin{aligned} T = T_w \quad at\ y = 0 \\ T \to T_\infty \ \ as\ \ y \to \infty \end{aligned}\right\} \tag{20}$$

Consider dimensionless temperature variable $\theta(\eta)$ of the form

$$\theta(\eta) = \frac{(T - T_\infty)}{(T_w - T_\infty)} \tag{21}$$

Using Eqs. (18), (19) and (21) in Eq. (15) we get non dimensional thermal boundary equations as

$$\frac{1}{Pr}\left(1 + \frac{4}{3}Nr\right)\theta'' + f\theta' + D_f\phi'' + \frac{MEc}{(1+m^2)}\left(f'^2 + g^2\right) + \frac{1}{Pr}(A^* f + B^*\theta) = 0 \tag{22}$$

$Pr = \frac{\mu c_p}{k}$ is the Prandtl number, $N_r = \frac{4\sigma^* T_\infty^3}{kK}$ is the dimensionless radiation coefficient, $D_f = \frac{Dk_t(C_w - C_\infty)}{\vartheta C_{sC_p}(T_w - T_\infty)}$ is the Dufour number, $Ec = \frac{U_s^2}{C_{p\Delta T}}$ is the Eckert number.

The corresponding non-dimensional boundary conditions for $\theta(\eta)$ reduce to

$$\left.\begin{aligned} \theta(\eta) = 1\ at\ \ \eta = 0 \\ \theta(\eta) = 0\ as\ \ \eta \to \infty \end{aligned}\right\} \tag{23}$$

The heat flux is given by

$$q_w = -k\frac{\partial T}{\partial y} \tag{24}$$

The local Nusselt number is given by

$$\mathrm{Nu_x} = \frac{x q_w}{k} \tag{25}$$

By using the non – dimensional variables Eqs. (7) and (21) in Eqs. (24) and (25), we get

$$\mathrm{Nu_x Re_x^{-1/2}} = -\theta'(0) \tag{26}$$

Mass transfer analysis:

The species concentration for the laminar boundary layer flow can be written as

$$u\frac{\partial C}{\partial x} + v\frac{\partial C}{\partial y} = D\frac{\partial^2 C}{\partial y^2}\frac{Dk_t}{T_m}\frac{\partial^2 C}{\partial y^2} - k_1(c - c_\infty) \tag{27}$$

where T_m is the mean fluid temperature, C_w is the uniform concentration and, C_∞ is the free stream concentration with $C_w > C_\infty$ and k_1 is the chemical reaction parameter.

The corresponding boundary conditions are given by

$$\left.\begin{aligned} C = C_w \quad at\ y = 0 \\ C \to C_\infty \ \ as\ \ y \to \infty \end{aligned}\right\} \tag{28}$$

We consider the non dimensional concentration variable

$$\phi(\eta) = \frac{(C - C_\infty)}{(C_w - C_\infty)} \tag{29}$$

Substitute Eq. (29) in Eq. (27), the ordinary differential equation of the mass concentration is obtained in the form

$$\phi'' + Sc(f\phi' + S_r\theta'' - \gamma\phi) = 0 \tag{30}$$

Where Sc = $\frac{\nu}{D}$ is the Schmidt number, $Sr = \frac{Dk_t(T_w - T_\infty)}{\vartheta T_m(C_w - C_\infty)}$ is the Soret number and $\gamma = \frac{k_1}{b}$ is the nondimensional chemical reaction parameter. It is pertinent to mention that $\gamma > 0$ corresponds to a destructive chemical reaction while $\gamma < 0$ indicates a generative chemical reaction.

The corresponding boundary conditions become

$$\left.\begin{aligned}\phi(\eta) = 1 \; at \;\; \eta = 0 \\ \phi(\eta) = 0 \; as \;\; \eta \to \infty\end{aligned}\right\} \tag{31}$$

The local Sherwood number is given by

$$\mathrm{Sh_x} = \frac{x q_m}{D} \tag{32}$$

The mass transfer coefficient may be written as follows:

$$q_m \;\; = \;\; -\mathrm{D}\frac{\partial C}{\partial y} \tag{33}$$

Here D is the molecular diffusivity

Using Eqs (7) and (29) in (32) and (33), we get

$$\mathrm{Sh_x Re_x^{-1/2}} = -\phi'(0) \tag{34}$$

METHOD OF SOLUTION:

An exact solution for f from Eqs. (8), (9), (22) and (30) together with the boundary conditions (7), (23) and (31) in the absence of Hall Currents, thermal buoyancy and solutal buoyancy can be obtained as

$$f(\eta) = f_w + \frac{1}{a}\left(1 - e^{-a\eta}\right), \qquad a = \frac{f_w + \sqrt{f_w^2 + 4(M + k_1 + 1)}}{2} \tag{35}$$

The set of non – linear coupled ordinary differential equations (8),(9), (22) and (30) with the boundary conditions (10), (23) and (31) are solved numerically employing the Runge – Kutta fourth order method together with the shooting technique. The boundary conditions as $\eta \to \infty$ enable us to use values of $f', g, \theta \; and \; \phi$ so that the velocity, temperature and concentration fields can easily be obtained for different variations in the physical parameters such as thermal buoyancy parameter, solutal buoyancy parameter, magnetic parameter, porous parameter, Prandtl number, thermal radiation parameter, Soret and Dufour numbers, Schmidt number, Eckert number and Chemical reaction parameter. The results are presented through several graphs and tables. In order to assure the accuracy of the numerical scheme the results are compared with those of Stanford Sateyi *et al.* [14] in the absence of chemical reaction, heat generation/absorption. The numerical results were compared with the exact solution for the skin friction $-f''(0)$ for various values of $k_p = 1/k_1$. Table 1 gives a comparison between the exact solution for the skin friction, the present numerical scheme, and results obtained by Stanford Sateyi *et al.* [21] and Elgazery [25] who used the Chebyshev pseudospectral method of solution. The following table shows an excellent agreement between our numerical results and the exact solution.

Table 1: Comparison of the skin friction, $-f''(0)$ with exact solution and those of Stanford Sateyi et al. and Elgazery for various values of K_p $\left(k_p = \frac{1}{k_1}\right)$ with $M = 1, m = \; Gr = Gc = A = \; B = r = Df = Sr = 0, Ec = 1, Pr = 0.72,$ $Sc = 1 \; and \; fw = -0.7$

k_p	Exact Solution	Present Method	Stanford Sateyi et al. [21]	Elgazery[25]
1	1.417059704707229	1.417059704272524	1.417059704707229	1.4170597047066027
2	1.269413474070165	1.269413473589358	1.269413474070165	1.2694134740920218
5	1.173975065412817	1.173975067409155	1.1739750656338466	1.1739750656338466
10	1.140805151587558	1.140805155666132	1.140805151587558	1.1408051520832996
15	1.129583274664413	1.129583279863610	1.1295832753169304	1.1295832753169304

RESULTS AND DISCUSSION

To obtain a physical insight of the problem, the profiles of velocity, temperature and concentration are graphically presented. The values of the parameters are fixed throughout the computations as $M = m = 1, G_r = G_c = 1,$ $k_1 = 1, p_r = 0.72,\ N_r = E_c = 1,\ D_f = S_r = 1,\ S_c = 1,\ \gamma = 1,\ f_w = 0.1,\ A^* = 0.01 = B^*$ unless otherwise stated.

Fig. (2) - (5) show the effect of the magnetic parameter on velocity, temperature and concentration. From fig. (2) it is evident that the influence of magnetic field is to diminish the velocity near the plate $(0 \leq \eta \leq 4)$ and outside this range the influence is negligible. This reduction can be attributed to the fact that the magnetic field provides a resisting type of force known as the Lorentz force. This force tends to lessen the motion of the fluid and as a consequence the velocity reduces. It is observed that the velocity along the sheet decreases with M accompanied by a reduction in the thickness of the boundary layer. From fig. (3) it is interesting to note that the magnetic parameter on the secondary velocity has an opposite effect to that on the primary velocity. It is seen that the velocity rapidly increases attaining its maximum value at $\eta = 1$ and then reduces in the remaining fluid region. From fig. (4) the temperature is found to enhance with magnetic field, the frictional resistance on account of the magnetic field results in the reduction of velocity and there by enhances the temperature in the thermal boundary layer. Hence, there is an increase in the thickness of thermal boundary layer. The effect of magnetic field on the concentration is very meager. However, it is observed that concentration increases slightly with increase in M. The influence of Hall parameter has a reversal effect to that of magnetic parameter on primary and secondary velocity, temperature and concentration.

The influence of the thermal buoyancy parameter λ on the flow variables is plotted in fig. (10) - (13). From fig. (10) it is noted that increasing values of the thermal buoyancy parameter has an enhancing effect on the primary velocity. We may conclude that the thermal buoyancy enhances the thickness of the boundary layer. The secondary velocity increases rapidly near the stretching surface attaining a maximum value around $\eta = 1$ and falls in the remaining region eventually attaining the zero value at far infinity. It is seen from figs. (12) and (13) that the effect of increasing thermal buoyancy parameter is to diminish temperature and concentration throughout the thermal and solutal boundary layers. This is attributed to the fact that an enhancement in the thermal buoyancy parameter results in the reduction of the thickness of the thermal and solutal boundary layers.

Figs. (14) - (17) display the influence of the solutal buoyancy number δ. It is noted that the velocity rises with increasing values of solutal buoyancy parameter. Further it is found that there is an overshoot of the velocity near the boundary for higher values of $\delta = 2.0$ and this peak value is diminished as δ decreases. The secondary velocity also increases with an increase in the solutal buoyancy parameter. The temperature and the mass concentration reduce for increasing values of δ which is attributed to the fact that the influence of increasing solutal buoyancy parameter δ is found to decrease the temperature and concentration as a result of the reduction in the thermal and solutal boundary layers thickness.

Figs. (22) - (25) illustrate the variation of Prandtl number. The primary velocity shows a reduction for increasing values of Prandtl number, away from the plate and hence the thickness of the boundary layer also reduces. The secondary velocity also behaves in a similar fashion as that of the primary velocity for a variation of Pr. As Prandtle number increases there is a significant reduction in the thermal boundary layer with a fall in the temperature throughout the boundary layer, since enhancement of Prantdtl number amounts to reduction of thermal diffusion. The mass concentration increases with Pr. However, the variation is very meager and as a result the thermal boundary layer also decreases mildly.

Figs. (18) - (21) display the plots of velocities, temperature and concentration distribution for various values of porous permeable parameter (k_1). It is seen that increasing values of the porous permeable parameter reduces primary velocity owing to the fact that the presence of porous medium enhances the resistance to the flow resulting in the reduction of velocity of fluid. The effect of porous permeable parameter on the secondary velocity is also similar. However, there is a significant reduction in the secondary velocity. The peak of the value of the secondary velocity when $k_1 = 3$ is less than half of its corresponding value when $k_1 = 1$. It is seen that the temperature increases with increasing values of k_1 as a result of the increase in the thickness of the thermal boundary layer owing to the Darcy drag developed by the porous medium.

The concentration is observed to increase on account of increase in the solutal boundary layer thickness for an increase in the value of the porous permeability parameter.

The variation of the thermal radiation parameter on the velocity, temperature and mass concentration is illustrated in figs. (26) - (29). It is observed that there is a significant rise in the primary velocity in the presence of thermal radiation throughout the boundary layer. Further increase in the values of the thermal radiation parameter results in the increase of the velocity. A similar behavior for the secondary velocity is also noticed with variation of the radiation parameter. However, the rise in the secondary velocity is noticed slightly away from the stretching surface. The radiation parameter is found to enhance the hydrodynamic boundary layers along x and y directions. The presence of thermal radiation is very significant on the variation of temperature. It is seen that the temperature increases rapidly in the presence of thermal radiation parameter throughout the thermal boundary layer. This may be attributed to the fact that as the Rosseland radiative absorption parameter R^* diminishes the corresponding heat flux diverges and thus rising the rate of radiative heat transfer to the fluid causing a rise in the temperature of the fluid. The thickness of the boundary layer also increases in the presence of Nr and further increases with increase in Nr. The effect of Nr on mass concentration is not significant as compared to temperature and velocity. However, the concentration decreases in the region $1 \leq \eta \leq 4$ for an increase in Nr.

Figs. (30) - (33) demonstrate the influence of the Eckert number on velocities, temperature and concentration. It is pointed out that the presence of Eckert number increases the temperature. This is due to the fact that the thermal energy is reserved in the fluid on account of friction heating. Hence, the temperature distribution rises in the entire thermal boundary layer. Further for higher values of $Ec \geq 3$ there is an overshoot of the temperature near the plate. The primary and secondary velocities are also found to enhance for increasing values of Ec owing to the energy release which increases the momentum. However, the mass concentration is to reduce marginally with increase in Ec.

Figs. (36) Illustrate the influence of space dependent heat source A^* on temperature distribution versus η in the thermal boundary layer. The presence of the heat source generates energy in the thermal boundary layer and as a consequence the temperature rises. Near the plate an overshoot in the temperature is also noticed. Increase in the values of $A^* > 0$ (heat source) produces further rise in the temperature. In the case of heat absorption $A^* < 0$ the temperature falls with decreasing values of $A^* < 0$ owing to the absorption of energy in the boundary layer. The influence of the heat generation is very meager on the primary velocity when compared to the secondary velocity. In either case both the velocities increase with increasing values of the heat generation parameter. The effect of the heat generation parameter is to reduce the mass concentration marginally.

Fig. (40) presents the influence of temperature dependent heat source / sink parameter B^* on temperature. As in the case of space dependent heat source the temperature increases due to the release of thermal energy for $B^* > 0$ while the temperature drops for decreasing values of $B^* < 0$ owing to the absorption of energy. The primary and secondary velocities increase for increasing values of the heat source parameter ($B^* > 0$) slightly away from the plate whereas for $B^* < 0$ the velocities decrease for decreasing values ofB^*. The effect of B^* on mass concentration is similar to that of A^*.

The effect of Dufour number (D_f) is illustrated in fig. (42) - (45). The primary velocity increases with increasing values of D_f. The same trend is observed for the secondary velocity also for increasing values of D_f. the temperature is found to increase with increasing values of D_f considerably. For $D_f > 0$ there is a overshoot of temperature. The thickness of the thermal boundary layer also increases effectively for increasing values of D_f. The mass concentration decreases nominally. We may conclude the Dufour parameter influence the temperature predominantly.

The variation of Soret parameter on velocities, temperature and mass concentration are plotted in fig. (46) - (49). It is seen that the primary and secondary velocities increase with increasing values of the Soret number. In contrast to the effect of D_f, the temperature decreases very nominally for increasing values of Sr. Similarly the mass concentration increases significantly for an increase in Soret parameter.

The influence of Schmidt number is given in fig. (50) - (53). The primary velocity and secondary velocity decrease with increasing values of Schmidt number, while the temperature increases throughout the thermal boundary layer. The mass concentration reduces very effectively with increasing values of Schmidt number.

Figs. (54) - (57) display the influence of chemical reaction parameter on velocities, temperature and concentration. It is observed that increasing values of the chemical reaction parameter show a reduction in the primary as well as secondary velocities. The temperature is observed to enhance for an increase in γ. The concentration decreases with chemical reaction parameter. In fact the concentration of the species steadily falls from its higher value on the surface to lower value eventually attaining the free stream concentration as $\eta \to \infty$.

From the table-2 it is observed that the skin friction coefficient decreases with increase in the magnetic parameter in view of the lesser momentum exerted on the wall with increasing values of M. The magnetic parameter increases the wall heat transfer rate. The Sherwood number at the wall diminishes with increasing values of M. The effect of the Hall parameter on the skin friction coefficient, heat transfer rate and Sherwood number is exactly opposite to that of the magnetic parameter M.

The porous parameter decreases the skin friction. The heat transfer rate at the wall enhances with increase in the porous parameter. The mass concentration rate also increases at the wall. Increasing values of Pr enhance the wall heat transfer rate. The variation of skin friction, Nusselt number and Sherwood number is plotted as function of Dufour number for different values of Soret number. It is observed from Fig. (58) that the skin friction coefficient increases with Dufour number and Soret number. The effect is significant for higher values of Dufour number. The Nusselt number also increases with increasing Soret number. The Sherwood number decreases with Dufour number. The effect of Sr in seen only for $D_f > 0.5$. It is significantly reduced for higher values of D_f and Sr.

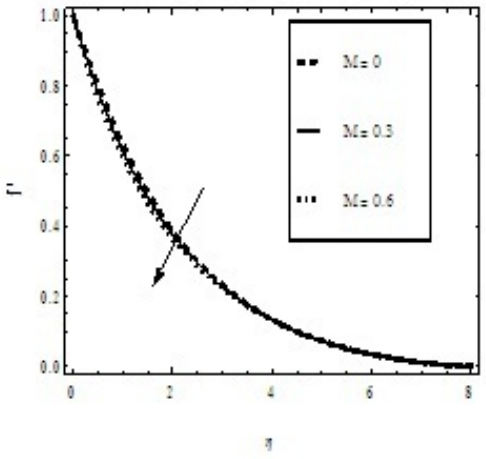

Fig. 2. Variation of $f'(\eta)$ with η for different values of M

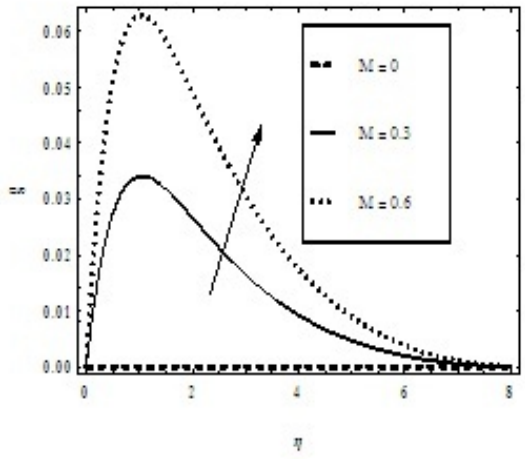

Fig. 3. Variation of $g(\eta)$ with η for different values of M

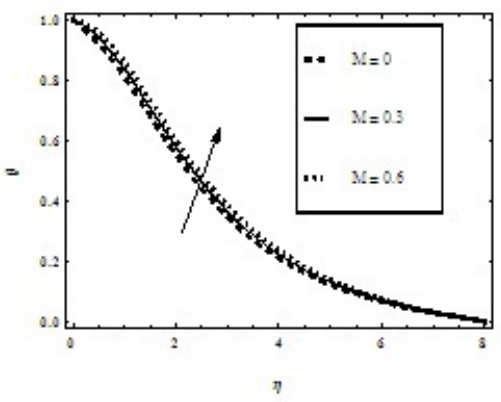

Fig. 4. Variation of $\theta(\eta)$ with η for different values of M

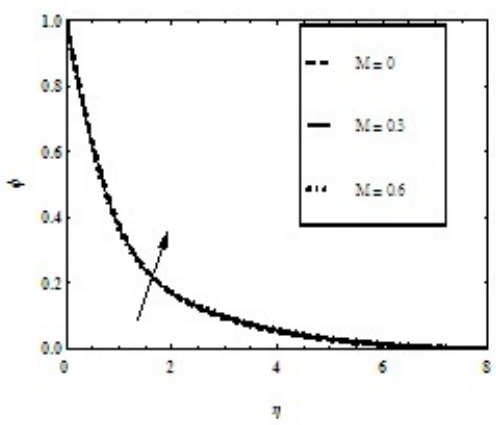

Fig. 5. Variation of $\phi(\eta)$ with η for different values of M

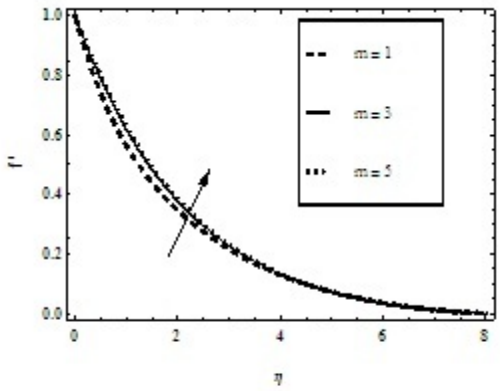

Fig. 6. Variation of $f'(\eta)$ with η for different values of m

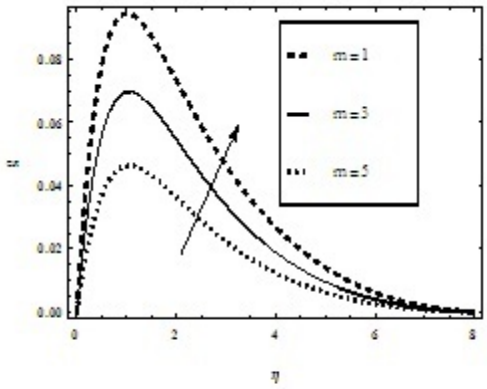

Fig. 7. Variation of $g(\eta)$ with η for different values of m

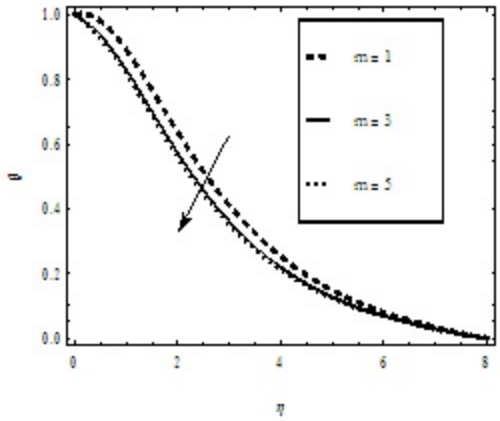

Fig. 8. Variation of $\theta(\eta)$ with η for different values of m

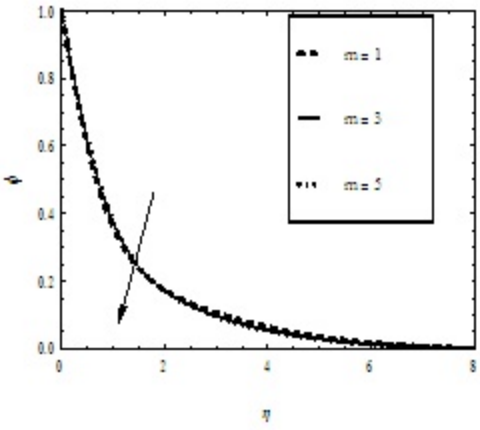

Fig. 9. Variation of $\phi(\eta)$ with η for different values of m

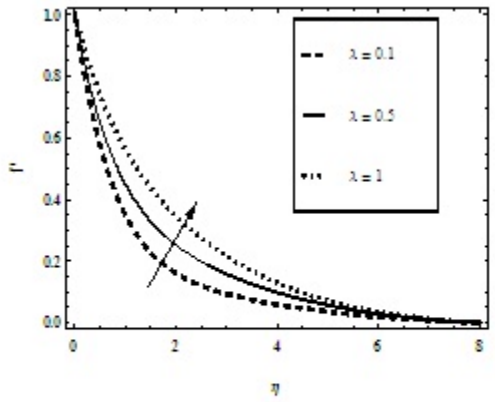

Fig. 10. Variation of $f'(\eta)$ with η for different values of λ

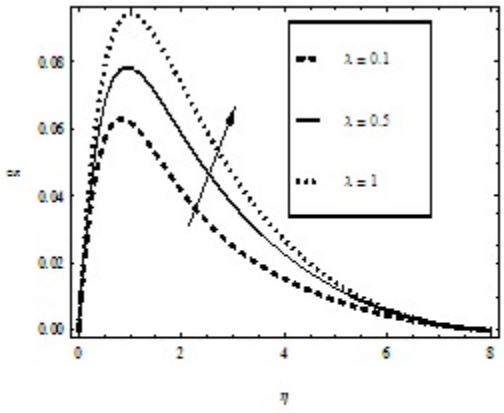

Fig. 11. Variation of g (η) with η for different values of λ

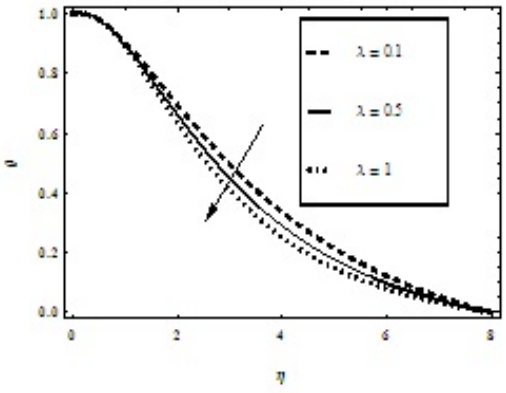

Fig. 12. Variation of $\theta(\eta)$ with η for different values of λ

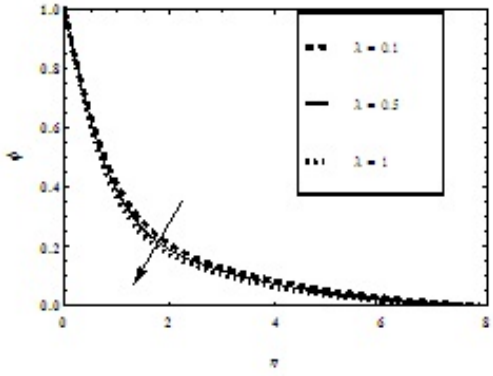

Fig. 13. Variation of $\phi(\eta)$ with η for different values of λ

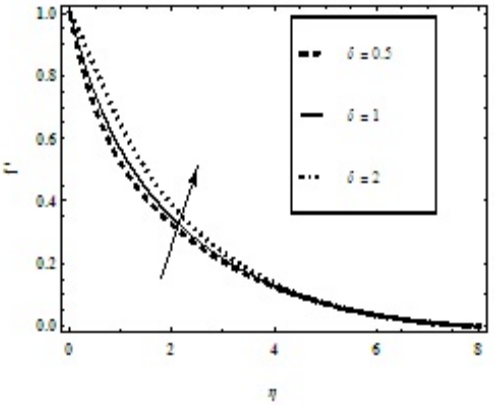

Fig. 14. Variation of $f'(\eta)$ with η for different values of δ

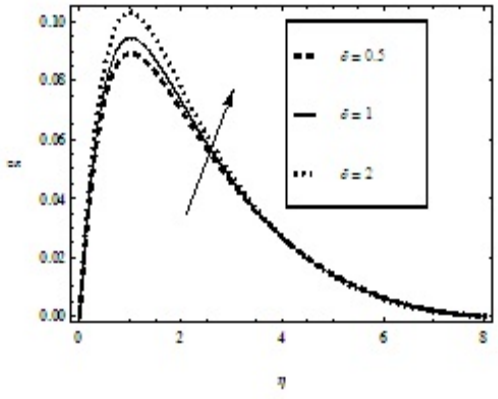

Fig. 15. Variation of $g(\eta)$ with η for different values of δ

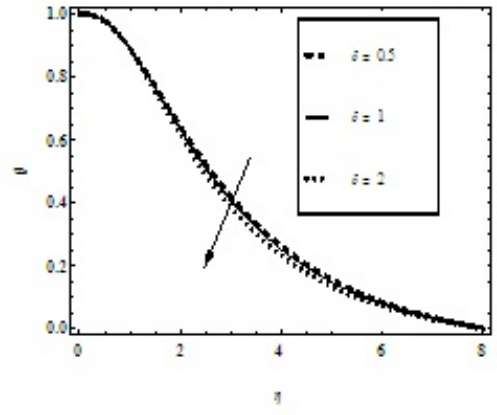

Fig. 16. Variation of $\theta(\eta)$ with η for different values of δ

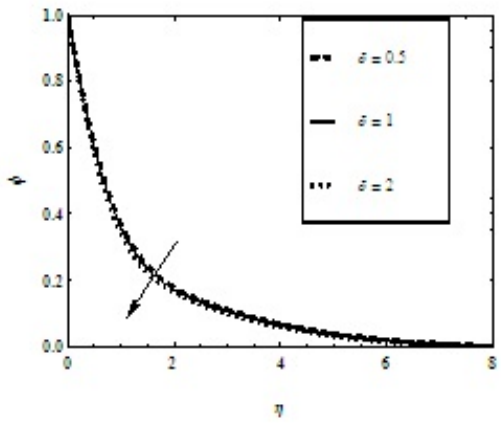

Fig. 17. Variation of $\phi(\eta)$ with η for different values of δ

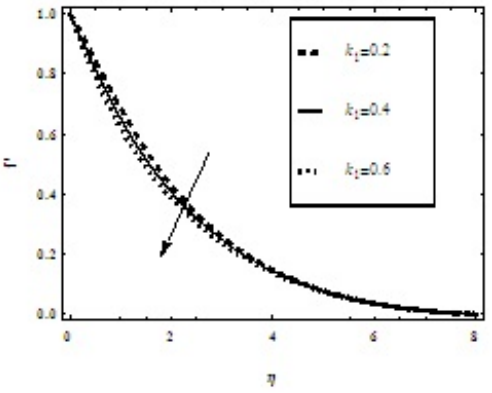

Fig. 18. Variation of $f'(\eta)$ with η for different values of k_1

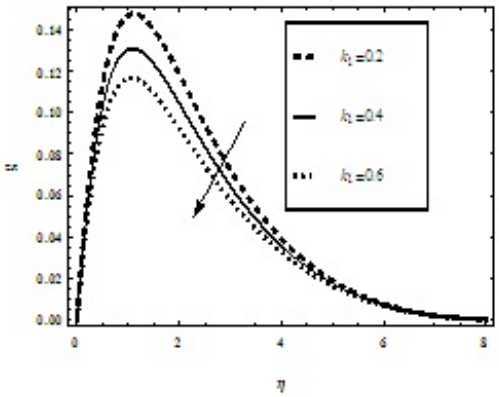

Fig. 19. Variation of $g(\eta)$ with η for different values of k_1

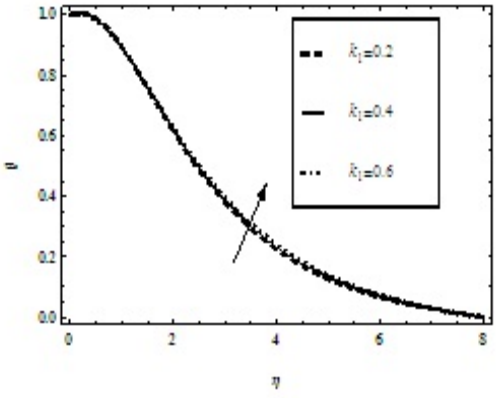

Fig. 20 Variation of $\theta(\eta)$ with η for different values of k_1

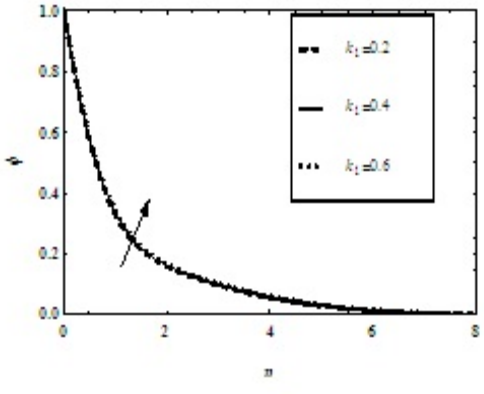

Fig. 21. Variation of $\phi(\eta)$ with η for different values of k_1

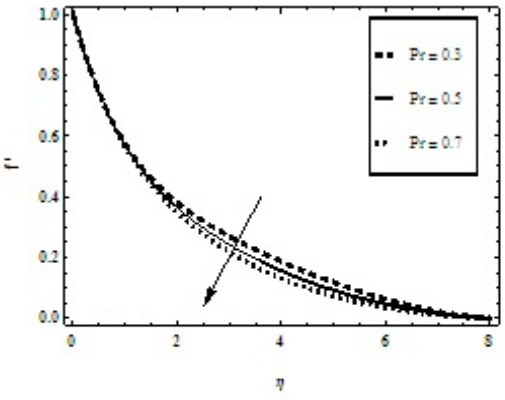

Fig. 22. Variation of $f'(\eta)$ with η for different values of Pr

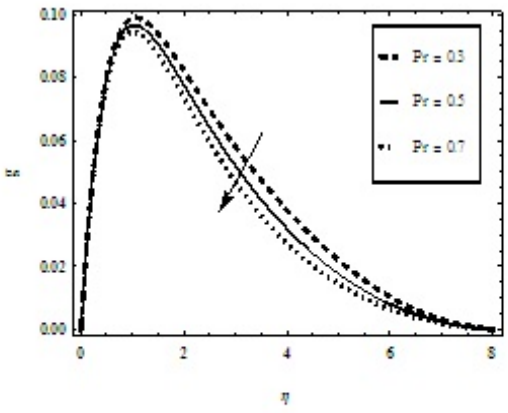

Fig. 23. Variation of $g(\eta)$ with η for different values of Pr

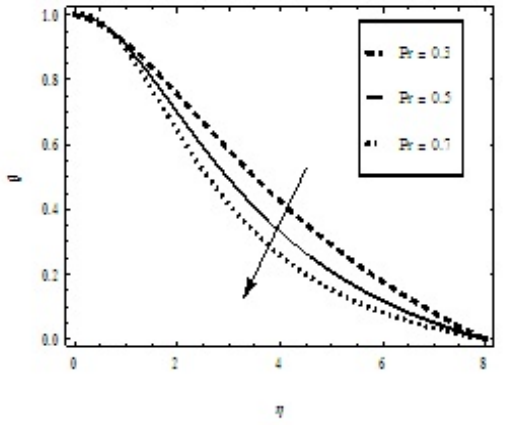

Fig. 24. Variation of $\theta(\eta)$ with η for different values of Pr

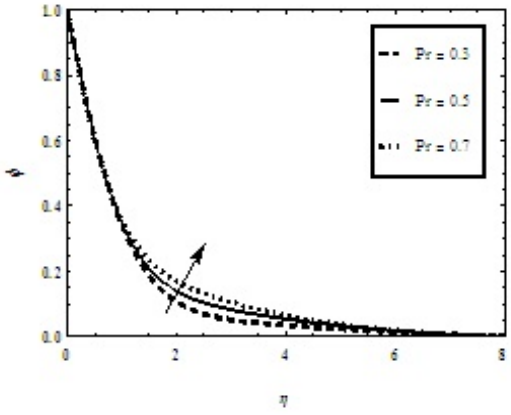

Fig. 25. Variation of $\phi(\eta)$ with η for different values of Pr

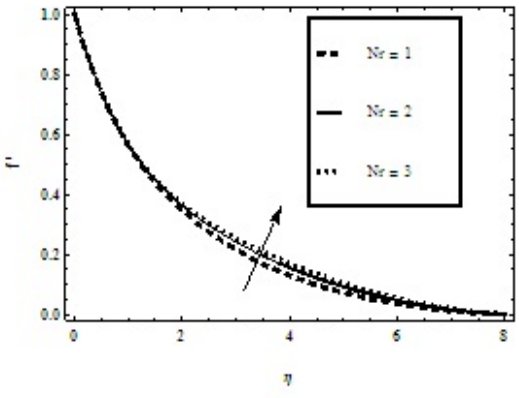

Fig. 26. Variation of $f'(\eta)$ with η for different values of Nr

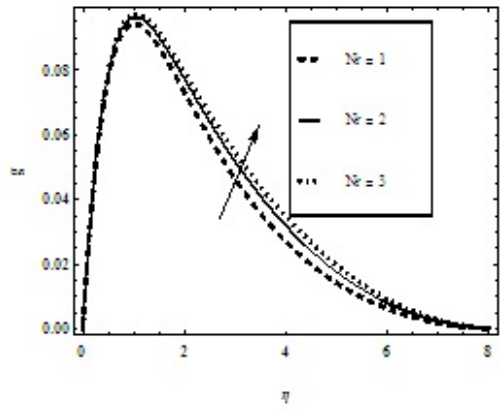

Fig. 27. Variation of $g(\eta)$ with η for different values of Nr

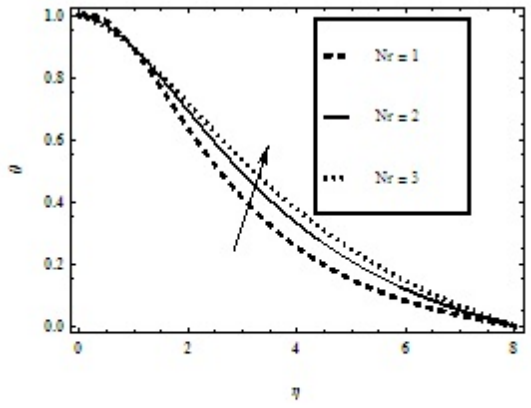

Fig. 28. Variation of $\theta(\eta)$ with η for different values of Nr

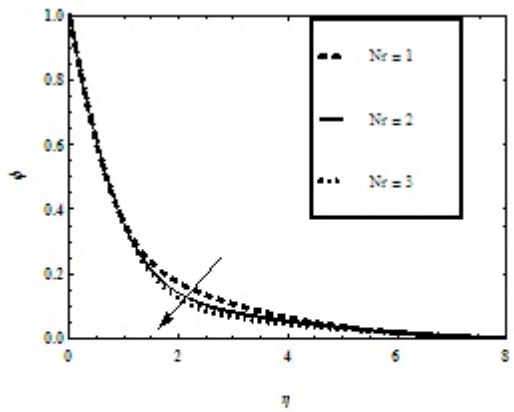

Fig. 29. Variation of $\phi(\eta)$ with η for different values of Nr

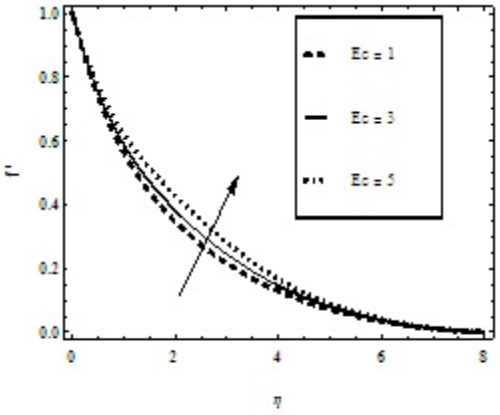

Fig. 30. Variation of $f'(\eta)$ with η for different values of Ec

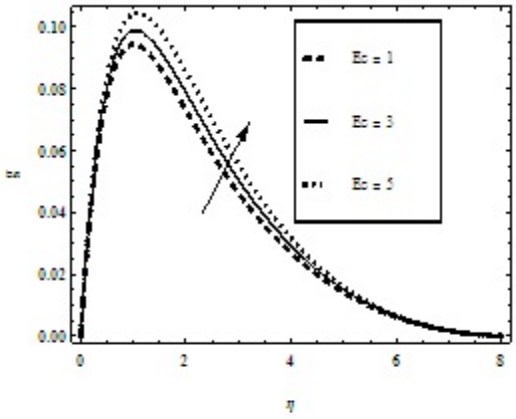

Fig. 31. Variation of $g(\eta)$ with η for different values of Ec

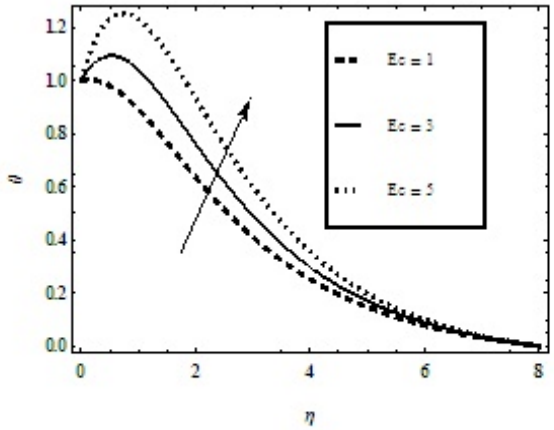

Fig. 32. Variation of $\theta(\eta)$ with η for different values of Ec

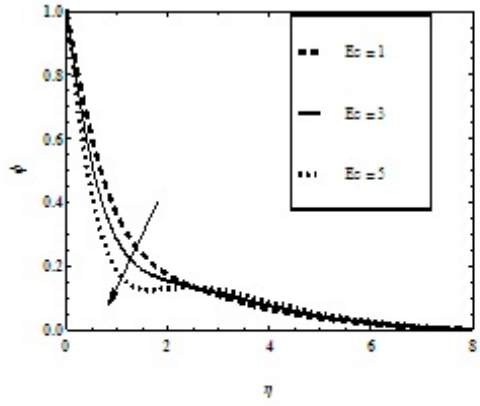

Fig. 33. Variation of $\phi(\eta)$ with η for different values of Ec

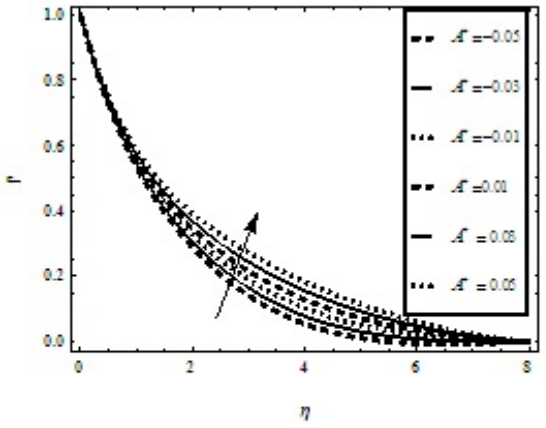

Fig. 34. Variation of $f'(\eta)$ with η for different values of A^*

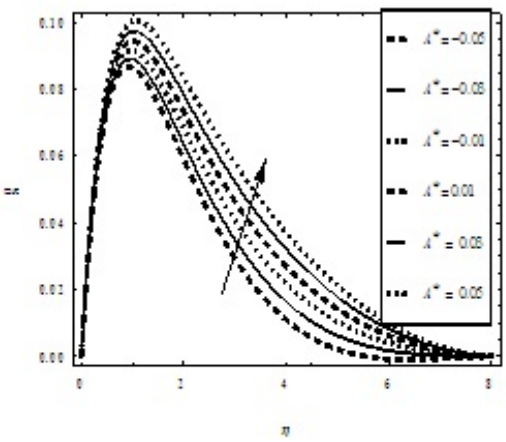

Fig. 35. Variation of $g(\eta)$ with η for different values of A^*

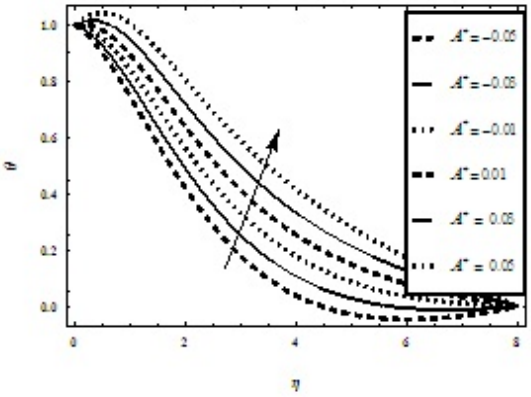

Fig. 36. Variation of $\theta(\eta)$ with η for different values of A^*

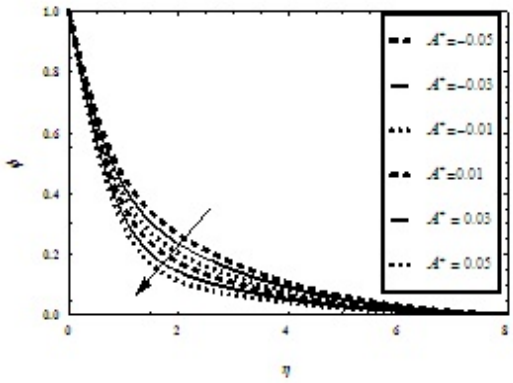

Fig. 37. Variation of $\phi(\eta)$ with η for different values of A^*

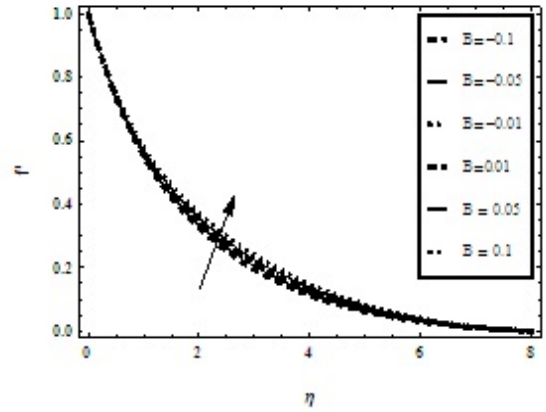

Fig. 38. Variation of $f'(\eta)$ with η for different values of B^*

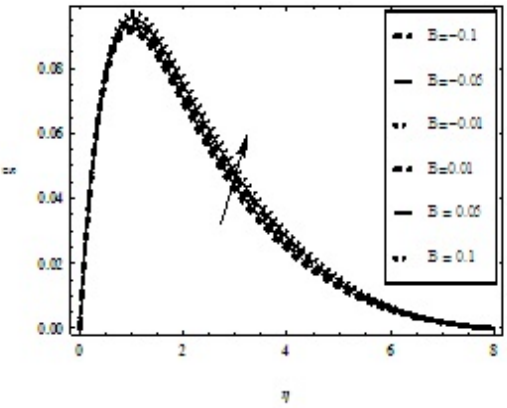

Fig. 39. Variation of $g(\eta)$ with η for different values of B^*

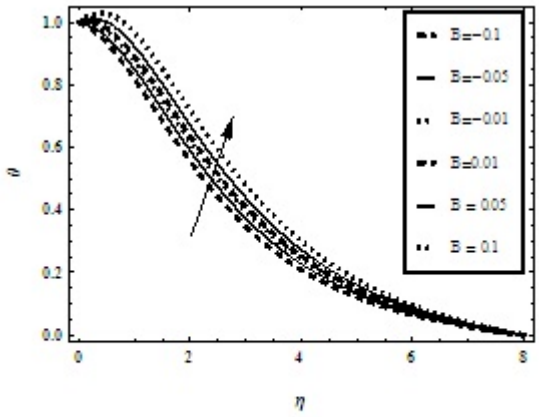

Fig. 40. Variation of $\theta(\eta)$ with η for different values of B^*

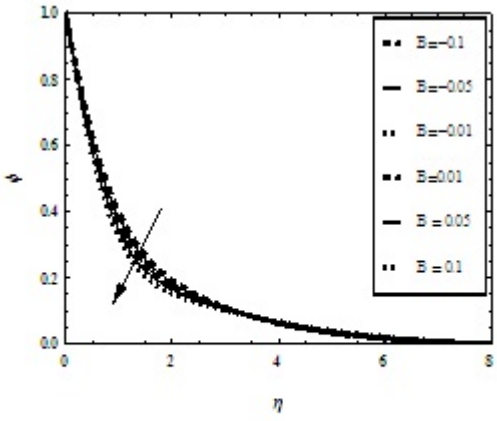

Fig. 41. Variation of $\phi(\eta)$ with η for different values of B^*

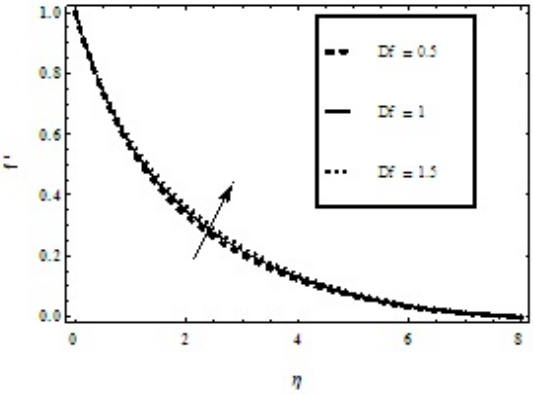

Fig. 42. Variation of $f'(\eta)$with η for different values of D_f

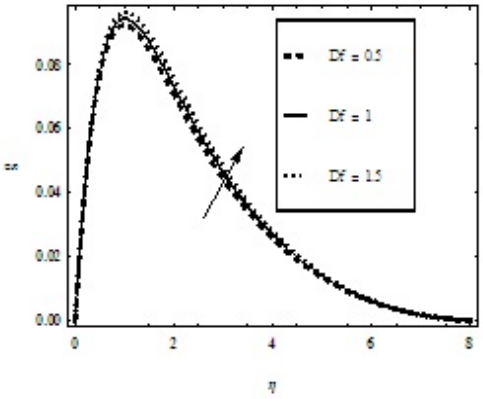

Fig. 43. Variation of $g(\eta)$with η for different values of D_f

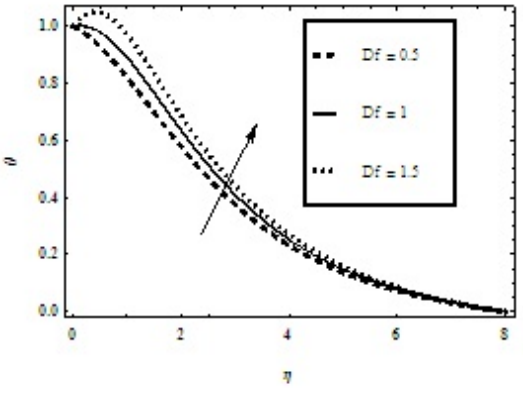

Fig. 44. Variation of $\theta(\eta)$ with η for different values of D_f

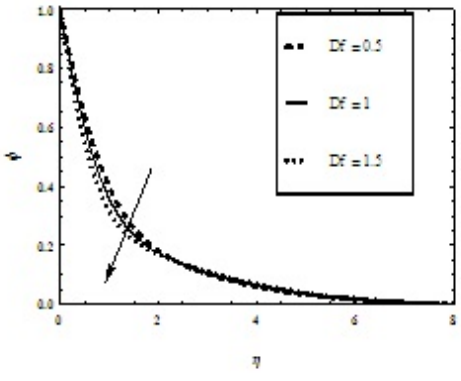

Fig. 45. Variation of $\phi(\eta)$ with η for different values of D_f

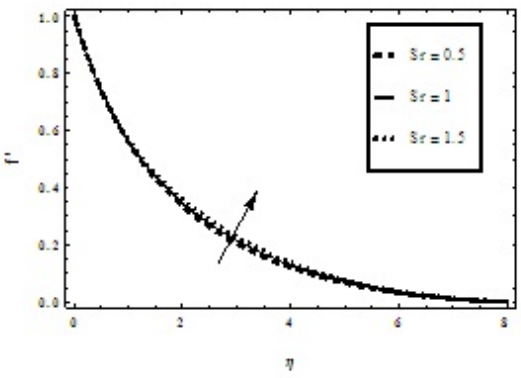

Fig. 46. Variation of $f'(\eta)$ with η for different values of S_r.

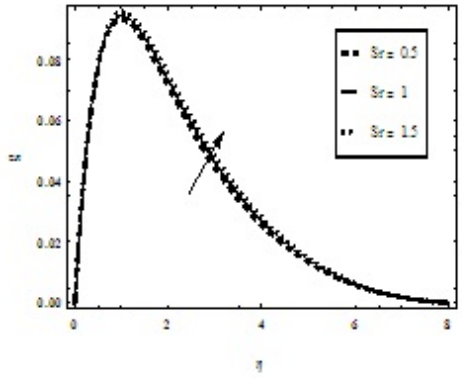

Fig. 47. Variation of $g(\eta)$ with η for different values of S_r.

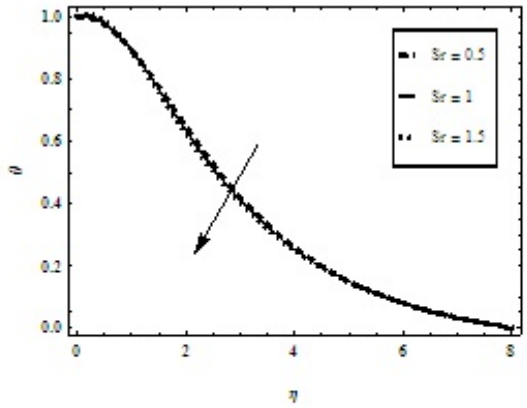

Fig. 48. Variation of $\theta(\eta)$ with η for different values of S_r.

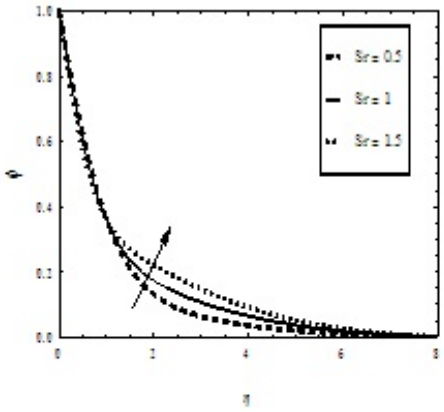

Fig. 49. Variation of $\phi(\eta)$ with η for different values of S_r.

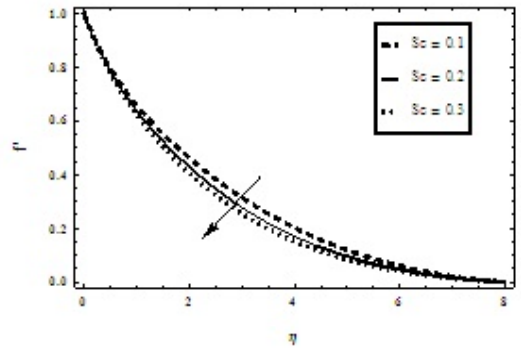

Fig. 50. Variation of $f'(\eta)$ with η for different values of Sc

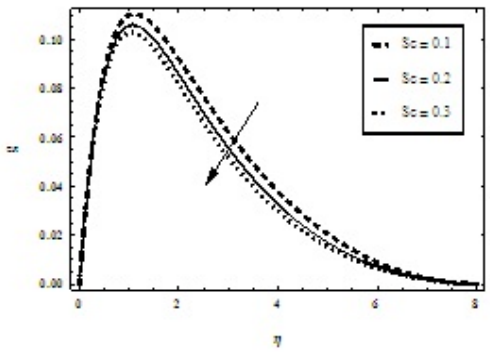

Fig. 51. Variation of $g(\eta)$ with η for different values of Sc

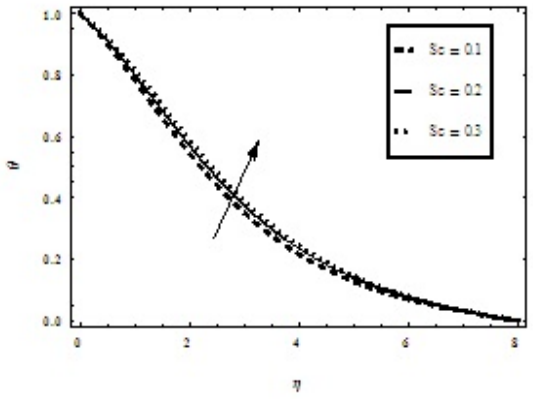

Fig. 52. Variation of $\theta(\eta)$ with η for different values of Sc

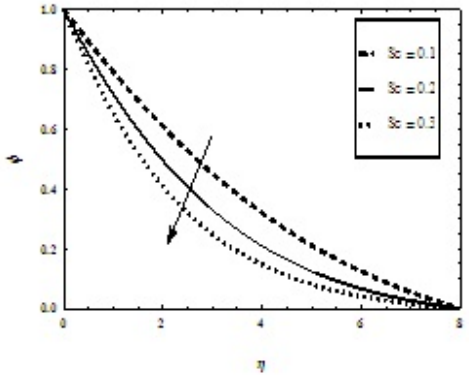

Fig. 53. Variation of $\phi(\eta)$ with η for different values of Sc

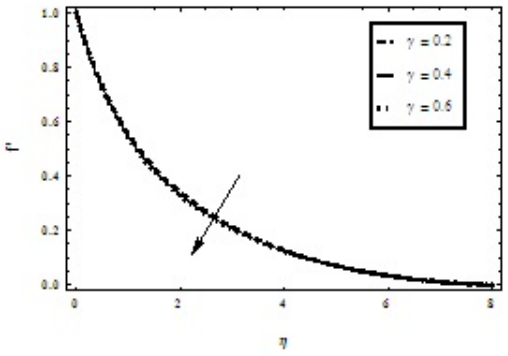

Fig. 54. Variation of $f'(\eta)$ with η for different values of γ

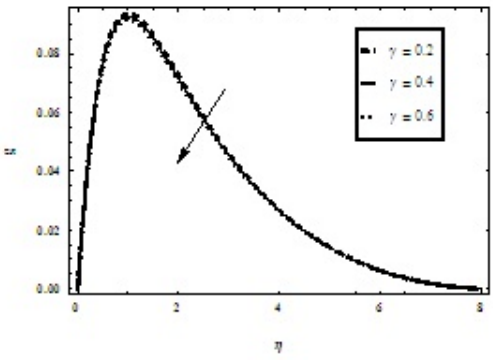

Fig. 55. Variation of $g(\eta)$ with η for different values of γ

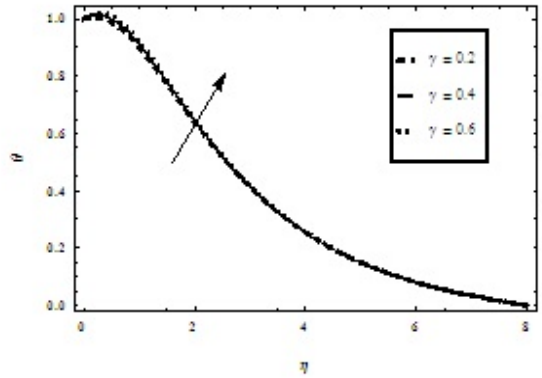

Fig. 56. Variation of $\theta(\eta)$ with η for different values of γ

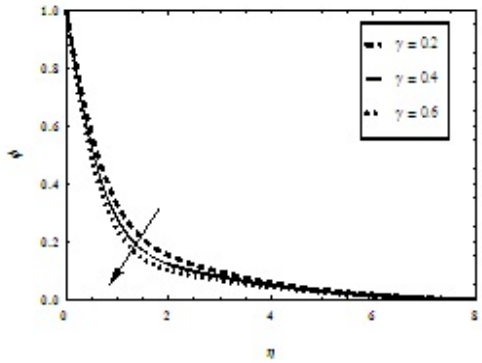

Fig. 57. Variation of $\phi(\eta)$ with η for different values of γ

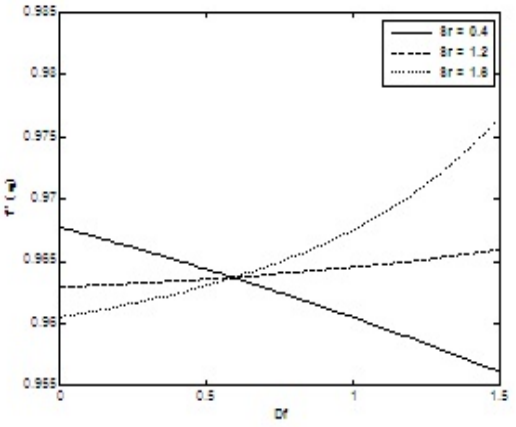

Fig. 58. Variations in skin-friction with D_f for different values of S_r.

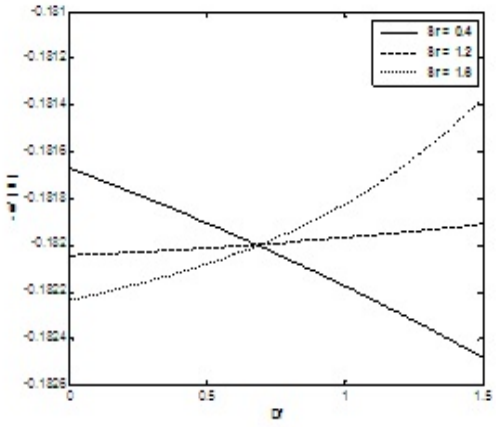

Fig. 59. Variations in local Nusselt number with D_f for different values of S_r.

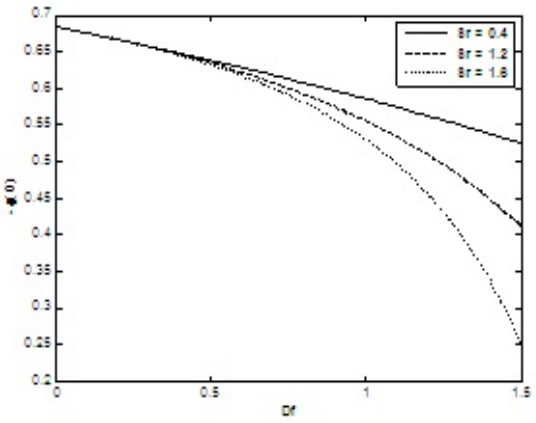

Fig. 60. Variations in local Sherwood number with D_f for different values of S_r.

Table-2: $C_{fx}Re_x^{1/2}, C_{fz}Re_x^{1/2}$, $Nu_xRe_x^{-1/2}$ *and* $Sh_xRe_x^{-1/2}$ for various values of $\mathrm{M, m}, \lambda, \delta, k_1, \mathrm{Pr, Nr}$, D_f, $\mathrm{Ec, Sc,\ sr}, \gamma, A^*, B^*$

M	m	??	??	??$_1$	Pr	Nr	??$_??$	Ec	Sc	Sr	??*	??*	??	fw	????$_??$????$_??^{-\frac{1}{2}}$ - $\theta(0)$	??h$_??$????$_??^{-\frac{1}{2}}$ - $\phi(0)$	??$_???$????$_??^{\frac{1}{2}}$??′(0)	??$_???$????$_??^{\frac{1}{2}}$?? (0)
0	1	1	1	1	0.72	1	1	1	1	1	0.01	0.01	1	0.1	-0.046692	1.475175	-0.474933	0.000000
0.3															-0.096040	1.504575	-0.542664	0.084505
0.6															-0.142621	1.531960	-0.611933	0.160883
1	1	1	1	1	0.72	1	1	1	1	1	0.01	0.01	1	0.1	-0.319112	1.640076	-0.882545	0.000000
	3														-0.200348	1.565486	-0.705165	0.251508
	5														-0.081160	1.494851	-0.527200	0.171253
1	1	0.1	1	1	0.72	1	1	1	1	1	0.01	0.01	1	0.1	-0.186552	1.518468	-1.252916	0.196318
		0.5													-0.177688	1.536143	-1.006643	0.222265
		1.0													-0.176970	1.559511	-0.713829	0.248711
1	1	1	0.5	1	0.72	1	1	1	1	1	0.01	0.01	1	0.1	-0.175024	1.551016	-0.864724	0.241704
			1.0												-0.176970	1.559511	-0.713829	0.248711
			2.0												-0.181634	1.576385	-0.416986	0.262069
1	1	1	1	0.2	0.72	1	1	1	1	1	0.01	0.01	1	0.1	0.0603362	-1.01789	-0.265922	0.343619
				0.4											0.053 5205	-1.00081	-0.367037	0.317873
				0.6											0.047773	-0.98506	-0.463391	0.295683
1	1	1	1	1	0.3	1	1	1	1	1	0.01	0.01	1	0.1	-0.007471	1.373472	-0.694528	0.256606
					0.5										-0.091114	1.457016	-0.699675	0.254079
					0.7										-0.189426	1.554714	-0.704694	0.251728
1	1	1	1	1	0.72	1	1	1	1	1	0.01	0.01	1	0.1	-0.200348	1.565486	-0.705165	0.251508
						2									-0.066245	1.435136	-0.699827	0.254320
						3									-0.012186	1.382871	-0.697452	0.255680
1	1	1	1	1	0.72	1	0.5	1	1	1	0.01	0.01	1	0.1	0.034938	1.391653	-0.725456	0.248022
							1								-0.200348	1.565486	-0.705165	0.251508
							1.5								-0.520351	1.814182	-0.683308	0.254971
1	1	1	1	1	0.72	1	1	1	1	1	0.01	0.01	1	0.1	-0.074979	1.567534	-0.702496	0.252387
								3							-0.498195	1.771424	-0.672057	0.257971
								5							-0.836019	1.999534	-0.633230	0.264941
1	1	1	1	1	0.72	1	1	1	0.1	1	0.01	0.01	1	0.1	0.138466	0.372334	-0.554754	0.272823
									0.2						0.090116	0.372334	-0.589060	0.266452
									0.3						0.048538	0.694448	-0.612878	0.262666

.

M	m	??	??	??$_1$	Pr	Nr	??$_??$	Ec	Sc	Sr	??*	??*	??	fw	????$_??$????$_??^{-\frac{1}{2}}$ - $\theta(0)$	??h$_??$????$_??^{-\frac{1}{2}}$ - $\phi(0)$	??$_???$????$_??^{\frac{1}{4}}$??′(0)	??$_???$????$_??^{\frac{1}{4}}$?? (0)
1	1	1	1	1	0.72	1	1	1	1	0.5	0.01	0.01	1	0.1	-0.147312	1.386937	-0.696690	0.251500
										1					-0.200348	1.565486	-0.705165	0.251508
										0.5					-0.278718	1.827135	-0.716206	0.251454
1	1	1	1	1	0.72	1	1	1	1	1	-0.05	0.01	1	0.1	-0.167630	1.542836	-0.708557	0.251093
											-0.03				-0.180897	1.551016	-0.706566	0.251518
											-0.01				-0.194288	1.559250	-0.704546	0.251950
											0.01				-0.207804	1.567534	-0.702496	0.252387
											0.03				-0.221447	1.575869	-0.700415	0.252830
											0.05				-0.235223	1.584261	-0.698304	0.253280
1	1	1	1	1	0.72	1	1	1	1	1	0.01	-0.1	1	0.1	-0.078030	-0.86422	-0.65684	0.256401
												-0.05			-0.027547	-0.90453	-0.65111	0.257781
												-0.01			0.015919	-0.93896	-0.64603	0.258997
												0.01			0.038806	-0.95698	-0.64331	0.259646
												0.05			0.087154	-0.99481	-0.63745	0.261036
												0.1			0.153045	-1.04584	-0.62924	0.262966
1	1	1	1	1	0.72	1	1	1	1	1	0.01	0.01	0.2	0.1	0.065357	-1.04801	-0.652942	0.258478
													0.4		0.111836	-1.20637	-0.66852	0.256623
													0.6		0.151995	-1.34229	-0.680675	0.255217

CONCLUSION

The problem of steady laminar hydro magnetic convective flow due to a stretching surface in the presence of Hall currents with Soret and Dufour effects is analyzed. The governing partial differential equations of the flow are transformed into ordinary differential equations by using similarity transformations. These equations are solved numerically by using the Runge – Kutta and shooting method for the evaluation of flow, heat and mass transfer, skin fricrion coefficient heat transfer and mass transfer. From the present analysis, the following conclusions are drawn:

1. Increasing values of the magnetic parameter retards the primary velocity and strongly enhances the secondary velocity.
2. The mixed convection parameter enhances the primary and secondary velocities.
3. The temperature and concentration are increased with an increase in the magnetic parameter.
4. The Hall parameter has an opposite influence on the velocities and temperature.
5. Increasing values of Eckert number produce a rise in the temperature with a overshoot of temperature near the surface for higher values of Eckert number.
6. The temperature increases with increase in the thermal radiation parameter and space dependent heat parameter as well as temperature dependent heat source parameter.
7. The Dufour number has an enhancing effect on the temperature while the Soret number has a reverse impact. The Prandtl number also has a reducing effect on temperature.
8. The primary and secondary velocities increase with increasing values of Dufour and Soret numbers.
9. The Chemical reaction parameter has a tendency to diminish the solute concentration in the solutal boundary layer.
10. The Soret number has a strong effect on mass concentration that it increases the concentration while the Dufour number has a reverse effect.
11. The skin friction coefficient and Nusselt number increase with increasing values of Soret number whereas reverse effect is seen on Sherwood number.
12. The Dufour effect increases skin friction coefficient and Sherwood number while a reverse trend is noticed for Nusselt number.
13. Higher values of Soret number and Dufour number have a strong influence on the Sherwood number.

REFERENCES

1. Salem A.M. and Abd El – Aziz M., Effect of Hall currents and chemical reaction on hydromagnetic flow of a stretching vertical surface with internal heat generation/absorption, Applied Mathematical Modeling 32(2008) 1236 – 1254.
2. M. S. Abel, N. Mahesha, Heat transfer in MHD viscoelastic fluid flow over a stretching sheet with variable thermal conductivity, non-uniform heat source and radiation, Appl. Math. Model. 32, 1965 (2008).
3. M. S. Abel, M. M. Nandeppanavar, Heat transfer in MHD viscoelastic boundary layer flow over a stretching sheet with non-uniform heat source/sink, Commun. Nonlinear Sci. Numer. Simul. 14, 2120 (2009).
4. A. Chakrabarti, A.S. Gupta, Hydromagnetic flow and heat transfer over a stretching sheet, Quart. Appl. Math. 37 (1979) 73.
5. P. Chandran, N.C. Sacheti, A.K. Singh, Hydromagnetic flow and heat transfer past a continuously moving porous boundary, Int. Commun. Heat Mass Transfer 23 (1996) 889.
6. T. Hayat, R. Ellahi, S. Asghar, Unsteady Magnetohydrodynamic Non-Newtonian Flow Due To Non-Coaxial Rotations of Disk and a Fluid At Infinity, Chem. Eng. Commun. 194, 37 (2007).
7. R. Ellahi, M. Hameed, Numerical analysis of steady non-Newtonian flows with heat transfer analysis, MHD and nonlinear slip effects,Int. J. Numer. Meth. Heat Fluid Flow. 22, 24 (2012).
8. R. Ellahi, The effects of MHD and temperature dependent viscosity on the flow of non-Newtonian nanofluid in a pipe: Analytical solutions, Appl. Math. Model. 37, 1451 (2013).
9. E.M. Abo-Eldahab, A.M. Salem, Hall effects on MHD free convection flow of a non-Newtonian power-law fluid at a stretching surface, Int. Commun. Heat Mass Transfer 31 (3) (2004) 343.

10. F. M. Ali, R. Nazar, N. M. Arifin, I. Pop, Effect of Hall current on MHD mixed convection boundary layer flow over a stretched vertical flat plate, Meccanica, October 2011, Volume 46, Issue 5, pp 1103-1112.
11. Knobloch, E. Convection in binary fluids. *Physics of Fluids*, 23, 1918–1920 (1980).
12. Taslim M. E. and Narusawa, U. Binary fluid convection and double diffusive convection in aporous medium. *Journal of Heat Transfer*, 108, 221–224 (1986).
13. D. Pal, H. Mondal, Commun. Nonlinear Sci. Numer. Simulat. 17 (2012) 672.
14. Anwar, B. O., Bakier, A. Y., and Prasad, V. R. Numerical study of free convection magnetohydrodynamic heat and mass transfer from a stretching surface to a saturated porous medium with Soret and Dufour effects. *Computational Materials Science*, 46, 57–65 (2009).
15. Sallam, N. Thermal diffusion and diffusion-thermo effects on mixed convection heat and mass transfer in porous medium. *Journal of Porous Media*, 13(4), 331–345 (2010).
16. Kuznetsov, A. V. and Nield, D. A. Double-diffusive natural convective boundary-layer flow of a nanofluid past a vertical plate. *International Journal of Thermal Sciences*, 50, 712–717 (2011).
17. R Kandasamy, K Periasamy and KKS Prabhu. Effects of chemical reaction, heat and mass transfer along a wedge with heat source and concentration in the presence of suction or injection. *Int. J. Heat Mass Tran*. 2005; 48, 1388-94.
18. MA Mansour, NF El-Anssary and AM Aly. Effects of chemical reaction and thermal stratification on MHD free convective heat and mass transfer over a vertical stretching surface embedded in a porous media considering Soret and Dufour numbers. *Chem. Eng. J*. 2008; 145, 340-5.
19. H.S. Takhar, A.J. Chamkha, G. Nath, Flow and mass transfer on a stretching sheet with a magnetic ®eld and chemically reactive speciesInt. J. Ther. Sci. 38 (2000) 1303.
20. A. NAYAK, S. PANDA, and D. K. PHUKAN, Soret and Dufour effects on mixed convection unsteady MHD boundary layer flow over stretching sheet in porous medium with chemically reactive species, *Appl. Math. Mech. - Engl. Ed.*, 35(7), 849–862 (2014) DOI 10.1007/s10483-014-1830-9.
21. Stanford Shateyi, Sandile Sydney Motsa and Precious Sibanda, The Effects of Thermal Radiation, Hall Currents, Soret, and Dufour on MHD Flow by Mixed Convection over a Vertical Surface in Porous Media, Hindawi Publishing Corporation Mathematical Problems in Engineering Volume 2010, Article ID 627475, 20 pages doi:10.1155/2010/627475.
22. R. C. Meyer, "On reducing aerodynamic heat transfer rates by magnetohydrodynamic techniques", Journal of the Aerospace Scienes, vol. 25, p. 561, 1958.
23. A. Raptis, Radiation and free convection flow through a porous medium, Int Comm Heat Mass Transfer, 25 (1998), pp. 289–295.
24. Dulal Pal, HiranmoyMondal, Soret and Dufour effects on MHD non-Darcian mixed convection heat and mass transfer over a stretching sheet with non-uniform heat source/sink, Physica B 407 (2012) 642–651.
25. N. S. Elagazery, "The effects of chemical reaction, Hall and ion-slip currents on MHD flow with temperature dependent viscosity and thermal diffusivity,' Communications in Nonlinear Science and Numerical simulation, vol. 14, no. 4, pp. 1267-1283, 2009.

Source of support: Nil, Conflict of interest: None Declared